Data, Innovation, and Science Cluster

Description of Algorithm

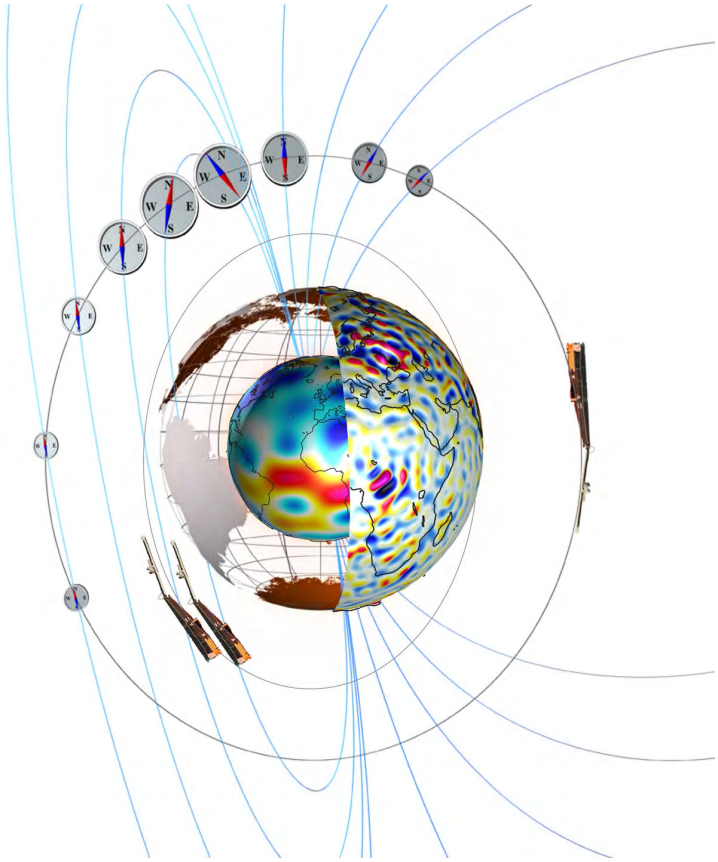

Doc.No: SW-DD-BCSS-GS-0001, Rev: 1A

Prepared:

Karl Magnus Laundal — Date 08–05–2019
Project Manager

Prepared:

Jone Peter Reistad — Date 08–05–2019

Approved:

Date 08–05–2019
Project Manager

Checked:

Date 08–05–2019

Record of changes

Reason	Description	Rev	Date
Issue 1	Initial version	rev 1	2018-04-17
Final release	Released by K. Laundal for publication	rev 1A	2019-05-07

Table of Contents

Preface

This document describes the details of how the *climatological model of ionospheric currents* is derived. The model is essentially a model of the magnetic field which is associated with the ionospheric currents. Section 1 describes the mathematical formulation that we use for the magnetic field, the data set that we use to constrain this formulation, and the inversion technique that is used. In Section 2 we clarify certain aspects regarding the interpretation of the model. In Section 3 we describe how ionospheric currents can be calculated from the model parameters. In that section we also describe an approach for relating the model magnetic field in space to ground perturbations.

1 Magnetic field model description

In this section we present 1) the mathematical representation that we have chosen for the disturbance magnetic field in space, above the horizontal ionospheric current layers, 2) the data set that we use to constain this representation, and 3) the details of how the model inversion is performed.

1.1 Mathematical formulation

The model formulation builds upon the description used by Laundal et al. [2016], the key parts of which are repeated here. The magnetic perturbation field, $\Delta\mathbf{B}$, can be represented as a sum of poloidal and toroidal parts [Backus, 1986, Olsen, 1997]:

$$\Delta\mathbf{B} = \Delta\mathbf{B}^{\text{pol}} + \Delta\mathbf{B}^{\text{tor}} = -\nabla V + \mathbf{r}\times\nabla T. \tag{1}$$

where V and T are scalar potentials that relate to the poloidal and toroidal parts of the magnetic field, respectively. These potentials we represent in terms of spherical harmonics:

$$V(\lambda_q, \phi_{\text{mlt}}, h) = R_E \sum_{n,m} \left(\frac{R_E}{R_E + h}\right)^{n+1} P_n^m(\theta_q)[g_n^m \cos(m\phi_{\text{mlt}}) + h_n^m \sin(m\phi_{\text{mlt}})], \tag{2}$$

$$T(\lambda_m, \phi_{\text{mlt}}) = \sum_{n,m} P_n^m(\theta_m)[\psi_n^m \cos(m\phi_{\text{mlt}}) + \eta_n^m \sin(m\phi_{\text{mlt}})], \tag{3}$$

where the spherical harmonic coefficients, g_n^m, h_n^m, ψ_n^m and η_n^m are functions of certain external parameters, to be described in more detail below. P_n^m are Schmidt semi-normalized Legendre functions of degree n and order m. R_E is the Earth's radius, and h is geodetic height. λ_q is quasi-dipole (QD) latitude, and λ_m is modified apex (MA) latitude. $\theta_q = 90° - \lambda_q$ and $\theta_m = 90° - \lambda_m$. QD and MA coordinates are variants of apex coordinate systems, defined by Richmond [1995]. The longitudinal parameter, ϕ_{mlt}, is the magnetic local time as defined by Laundal and Richmond [2017], using QD/MA longitudes (these are always equal). QD and MA coordinates are non-orthogonal, and so evaluation of (1) involves base vectors which depend on the local structure of the Earth's main magnetic field. The relevant base vectors are called $\mathbf{f}_i$ and $\mathbf{d}_i$ below, and they are calculated using code published by Emmert et al. [2010][1]. We use the following expressions [Laundal et al., 2016] for the geodetic eastward (subscript e), northward (n) and upward (u) components, respectively:

[1] This code is accessed through the Python wrapper available at https://github.com/cmeeren/apexpy

$$\begin{aligned}\Delta B_e =& \frac{-d_{1,n}}{\cos\lambda_m}\frac{\partial T}{\partial \phi_{\text{mlt}}} \\ &+ \frac{d_{2,n}}{\sin I_m}\frac{\partial T}{\partial \lambda_m} \\ &- \frac{f_{2,n}}{R_E+h}\frac{1}{\cos\lambda_q}\frac{\partial V}{\partial \phi_{\text{mlt}}} \\ &+ \frac{f_{1,n}}{R_E+h}\frac{\partial V}{\partial \lambda_q} \end{aligned} \tag{4}$$

$$\begin{aligned}\Delta B_n =& \frac{d_{1,e}}{\cos\lambda_m}\frac{\partial T}{\partial \phi_{\text{mlt}}} \\ &- \frac{d_{2,e}}{\sin I_m}\frac{\partial T}{\partial \lambda_m} \\ &+ \frac{f_{2,e}}{R_E+h}\frac{1}{\cos\lambda_q}\frac{\partial V}{\partial \phi_{\text{mlt}}} \\ &- \frac{f_{1,e}}{R_E+h}\frac{\partial V}{\partial \lambda_q} \end{aligned} \tag{5}$$

$$\Delta B_u = -\sqrt{F}\frac{\partial V}{\partial h} \tag{6}$$

where[2]

$$\sin I_m = \frac{2\sin\lambda_m}{\sqrt{4-3\cos^2\lambda_m}}. \tag{7}$$

Equations 1−7 relate the magnetic field $\mathbf{\Delta B}$ to the spherical harmonic coefficients, h_n^m, g_n^m, η_n^m, and ψ_n^m. In the model presented here, these spherical harmonic coefficients are functions of external parameters. Each coefficient is written in terms of 19 other coefficients. Using g_n^m as an example, the expansion that we use is:

$$\begin{aligned} g_n^m =& g_{n1}^m + g_{n2}^m\sin\theta_c + g_{n3}^m\cos\theta_c + g_{n4}^m\epsilon + g_{n5}^m\epsilon\sin\theta_c + g_{n6}^m\epsilon\cos\theta_c + \\ & g_{n7}^m\beta + g_{n8}^m\beta\sin\theta_c + g_{n9}^m\beta\cos\theta_c + g_{n10}^m\beta\epsilon + g_{n11}^m\beta\epsilon\sin\theta_c + g_{n12}^m\beta\epsilon\cos\theta_c + \\ & g_{n13}^m\tau + g_{n14}^m\tau\sin\theta_c + g_{n15}^m\tau\cos\theta_c + g_{n16}^m\beta\tau + g_{n17}^m\beta\tau\sin\theta_c + g_{n18}^m\beta\tau\cos\theta_c + \\ & g_{n19}^m \mathrm{F}_{10.7}. \end{aligned} \tag{8}$$

Here

$$\theta_c = \arctan2(B_y, B_z) \tag{9}$$

is the IMF clock angle, which depends on the GSM y and z components of the interplanetary magnetic field (nT is consistently used as a unit for magnetic fields). β is the dipole tilt angle in degrees, and ϵ is the Newell et al. [2007] coupling function,

$$\epsilon = 10^{-3}|v_x|^{4/3}\sqrt{B_y^2+B_z^2}^{2/3}\sin^{8/3}(\theta_c/2). \tag{10}$$

v_x is the GSM (or GSE) x component of the solar wind velocity, in km/s. We also define a quantity

$$\tau = 10^{-3}|v_x|^{4/3}\sqrt{B_y^2+B_z^2}^{2/3}\cos^{8/3}(\theta_c/2), \tag{11}$$

[2]There is a typo in the corresponding equation in the paper by Laundal et al. [2016], where $\cos\lambda_m$ is not squared.

which is similar to ϵ, only that it maximizes for purely northward IMF instead of southward IMF. Finally, $F_{10.7}$ is an index of the 10.7 cm radio flux coming from the Sun, a much used proxy for the intensity of ionizing EUV radiation. The unit for $F_{10.7}$ is "solar flux units" (SFU). Pre-processing of these external parameters is described in more detail in the next section (1.2).

Equations 1−11 can be combined to relate the magnetic disturbance field, $\mathbf{\Delta B}$, to the coefficients $h^m_{n,i}, g^m_{n,i}, \eta^m_{n,i}$, and $\psi^m_{n,i}$, $i = 1, 2, \ldots, 19$. The total number of coefficients depends on the truncation levels chosen in Equations 2 and 3. We choose $N_V, M_V = 45, 3$, and $N_T, M_T = 65, 3$, which leads to a total of 758 terms in the spherical harmonic representations, each of which depends on 19 parameters (Equation 8). In total, the model has 14,402 parameters.

1.2 The data

The parameters are estimated by use of magnetic field measurements from the CHAMP and *Swarm* satellites.

We use vector measurements, with main field model predictions [Finlay et al., 2016] subtracted. The main field model includes the magnetic field of the Earth's core and crust, and an estimate of the large-scale magnetospheric (basically the symmetric ring current) field. The remaining field is presumably associated with ionospheric currents: Polar and equatorial electrojets, Birkeland currents, and solar quiet currents. We use low Earth orbit 1 Hz measurements, sampled at 30 second cadence. The CHAMP data are from August 2000 to September 2010. *Swarm* data are from December 2013 to August 2016. The only selection criterion is that the coinciding external parameter is available (see details below). Possible outliers are handled in the inversion step (see 1.3).

Swarm Alpha and Charlie fly side-by-side. For our purposes, their measurements are not statistically independent, and so they are weighted by 0.5 in all the following statistics, including the model parameters.

Solar wind measurements are obtained from OMNI 1-min values[3]. As a pre-processing step, we calculate the mean of these measurements based on the 20 preceding minutes. If no data is available during that period, the data point is discarded. A justification for this is given in Section 2.

F10.7 is provided on a daily basis[4]. The daily values are linearly interpolated to the times of the satellite measurements.

The dipole tilt angle is calculated at the time of the satellite measurements, using equation 15 from Laundal and Richmond [2017].

In total, we have 16,839,394 vector measurements, and three times as many components. The solution will be dominated by the most frequently appearing external values, so therefore we plot their distribution in Figure 1. Alpha and Charlie data points are attributed half weight in these distributions.

[3] Available from https://omniweb.gsfc.nasa.gov/ow_min.html
[4] Available from http://lasp.colorado.edu/lisird/

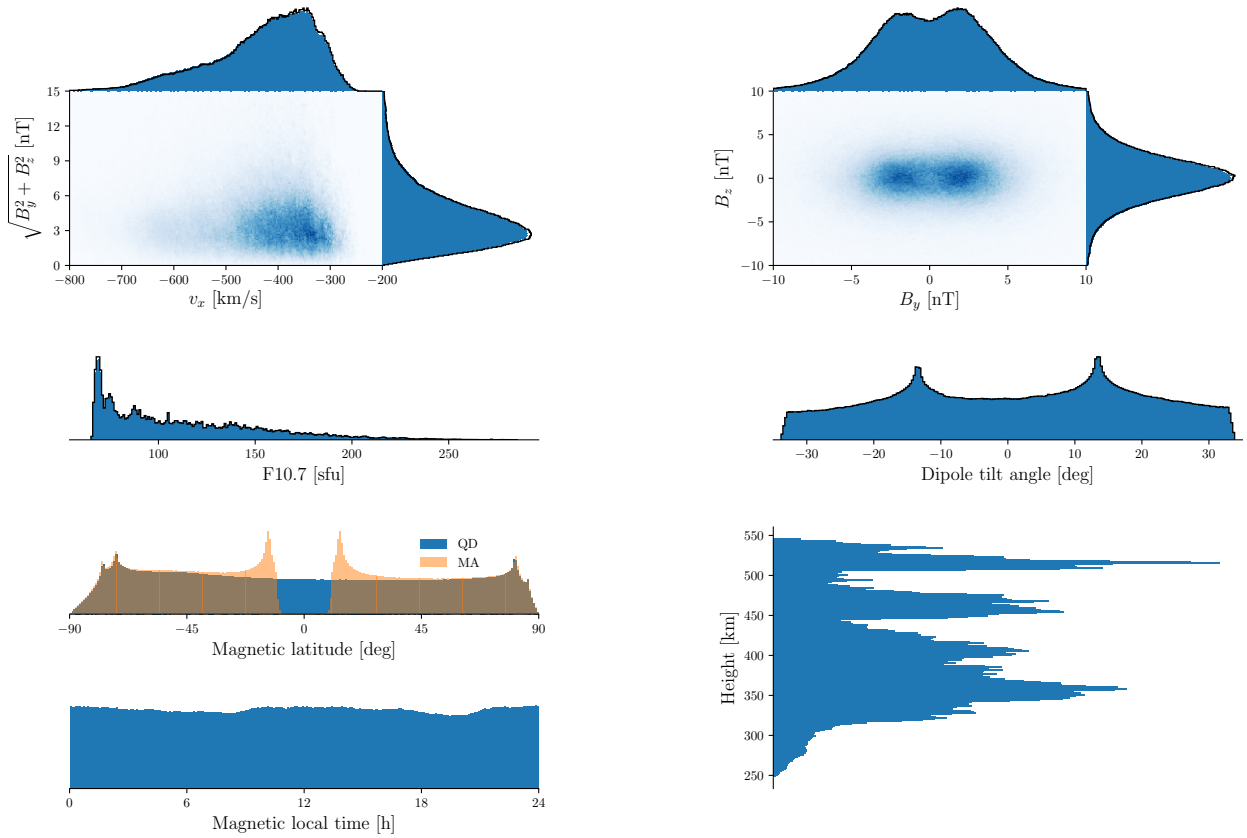

Figure 1: Histograms showing how the data points used to make the model are distributed with respect to different variables and coordinates, denoted by axis labels. Each histogram is based on 16,839,394 points, except for the solar wind plots which are truncated at the extreme ends of the distributions. Measurements from *Swarm* Alpha and Charlie are weighted by 0.5 in these plots. In the 2D plots, increasingly dark blue color denotes more frequent values.

1.3 Inversion

Estimating the model parameters essentially corresponds to solving the inverse problem

$$\mathbf{Gm} = \mathbf{d} \tag{12}$$

where $\mathbf{m}$ is a column vector with the 14,402 model parameters, $h^m_{n,i}, g^m_{n,i}, \eta^m_{n,i}, \psi^m_{n,i}$. $\mathbf{d}$ is a column vector of measured eastward, northward, and upward components, 50,518,182 elements in total. $\mathbf{G}$ is the design matrix, with $D = 50,518,182$ rows and $U = 14,402$ columns, which relate the model parameters to the measurements, according to equations 1−11.

This over-determined set of equations is solved by iteratively re-weighted least squares, explained here in detail. First, we multiply equation 12 by a $D \times D$ weight matrix $\mathbf{W}^s$, whose elements are zero except at the diagonal where they are 1 at the rows corresponding to CHAMP and *Swarm* Bravo measurements, and 0.5 at the rows corresponding to *Swarm* Alpha and Charlie measurements. This weighting is introduced because Alpha and Charlie fly side by side, and are assumed not to provide independent measurements at the scales resolved by the model. Then we multiply the equation by $\mathbf{G}^\top$. An initial solution can be written as

$$\mathbf{m}_0 = (\mathbf{G}^\top \mathbf{W}^s \mathbf{G} + \mathbf{R})^{-1} \mathbf{G}^\top \mathbf{W}^s \mathbf{d}. \tag{13}$$

Here we have also introduced an $U \times U$ regularization matrix $\mathbf{R}$. The regularization matrix is zero everywhere except at the diagonal elements corresponding to $\psi^m_{n,i}$ and $\eta^m_{n,i}$. These elements are $\kappa^2 n(n+1)/(2n+1)$, where κ^2 is a regularization parameter. Equation 13 is solved using Cholesky decomposition, using the Python Scipy library, which calls the LAPACK library [Anderson et al., 1999]. This is only possible if $\mathbf{G}^\top \mathbf{W}^s \mathbf{G} + \mathbf{R}$ is positive definite. We choose the smallest value for the regularization parameter κ^2, in powers of 10, for which $\mathbf{G}^\top \mathbf{W}^s \mathbf{G} + \mathbf{R}$ is positive definite. No regularization is needed for the poloidal field parameters. The need for regularization in the toroidal parameters probably has to do with the facts that 1) modified apex coordinates do not cover the whole globe at satellite height (equatorial latitudes are missing, as seen in Figure 1), and 2) near the equator the latitudinal variation of T is not well constrained (see equations 5 and 4), since $d_{2,e}$ and $d_{2,n}$ are very small there. While T will be defined at low latitudes, we do not expect it to be physically meaningful there (meaning that field-aligned currents at low latitudes are not resolved).

In the next steps, we introduce an additional set of weights according to the data misfit in the previous iteration. With $\mathbf{m}_j$ as the solution of the j'th iteration, we calculate residuals, $\mathbf{e}_j = \mathbf{d} - \mathbf{G}\mathbf{m}_j$. Based on these, a set of Huber weights [Huber, 1964] is calculated,

$$w^i_j = \min(1, 1.5\sigma_j / |e^i_j|) \tag{14}$$

where e^i_j is the i'th elements in $\mathbf{e}_j$. σ_j is the root mean square of the elements in $\mathbf{e}_j$, where the mean is also calculated robustly, using iterative re-weighting by Huber weights. The $(j+1)$'th iteration for the model parameter vector can be written

$$\mathbf{m}_{j+1} = (\mathbf{G}^\top \mathbf{W}^h_j \mathbf{W}^s \mathbf{G} + \mathbf{R})^{-1} \mathbf{G}^\top \mathbf{W}^h_j \mathbf{W}^s \mathbf{d}. \tag{15}$$

where $\mathbf{W}^h_j$ is a diagonal weight matrix of Huber weights, calculated by (14) using the residuals from the j'th iteration. The final solution is achieved when $\|\mathbf{m}_{j-1} - \mathbf{m}_j\| < 10^{-2}\|\mathbf{m_0}\|$.

This iterative technique reduces the effect of outliers, so that the final solution better represents typical values, which may be different from the plain mean. The currents will typically be weaker and smoother in later iteration steps than they are in the first step. The black contours in Figure 1 show the distributions of the external parameters for the input, weighted by the final set of Huber weights found by following the scheme described above. It is clear that the black contours are not significantly different from the distributions shown in blue, which are not Huber-weighted. If they were different, it would indicate that the model formulation was valid only for typical conditions, and that other functional relationships are more suitable at extreme values. We conclude that the model formulation is generally appropriate.

2 A note about model interpretation

The model represents the **global average** ionospheric disturbance magnetic field associated with the **direct** interaction between the magnetosphere, whose state is described by the dipole tilt angle[5], and the solar wind (described by its speed in the GSM x direction) and the interplanetary magnetic field (described by its components in the GSM yz plane). A detailed discussion of this interpretation belongs in a scientific publication. However, since it directly impacts the choice of parametrization and data pre-processing, some aspects of the interpretation are discussed below.

First, the model should be regarded as an "equation of state" rather than a dynamic description of the magnetic field and currents. It can be used to analyze average configurations of the current systems, but not dynamical changes. We emphasize that the true current system is strongly structured in space and time, while this model only captures the quasi-static large-scale variations.

The choice of parametrization in equation 8 dictates which processes whose effect the model can describe. The processes are subsolar reconnection, which is assumed to be proportional to ϵ [Newell et al., 2007], and lobe reconnection, which is assumed to be proportional to τ. The reconnection effects are also dependent on the IMF clock angle and on the seasons. Combining the solar wind and IMF parameters to ϵ and τ is a key difference from the parametrization used by Weimer [2013]. Another key difference is that we include multiplicative cross terms between the parameters. This prevents one parameter from completely overshadowing the others during extreme conditions, unless the data dictates such a behaviour. For example, in Weimer's model there will, a priori, be negligible seasonal variations when the solar wind speed is large, since the terms containing dipole tilt and solar wind speed are completely decoupled.

In order to interpret the model as the average effect of dayside reconnection, it is important that the input represents the instantaneous solar wind/IMF impacting the magnetopause. Naively, this suggests using as high time resolution input as possible. However, it is probably more appropriate to use some time averaging of the input, since 1) in situ high resolution measurements of the solar wind may not be a good representation of its large-scale structure due to spatial variations/turbulence, and 2) the time shift from the solar wind monitor to the magnetopause will be imperfect (we use the time shift given by OMNI, which propagates the measurements to the bow shock). These effects can likely be reduced by low-pass filtering (time averaging). However, increasing the window for temporal averaging will lead to another complication: The dayside and nightside reconnection rates will become increasingly well correlated. We want to avoid this, in order to have a clear physical interpretation of the model in terms of dayside processes.

As a trade-off between these effects, we have chosen an averaging window of 20 min for the solar wind IMF measurements, covering the time prior to the time of the associated LEO measurement. That means that, if $x(t)$ is the OMNI 1-min solar wind parameter at time t, we use $\overline{x}(t) = \int_{t-20}^{0} \frac{x(t)}{20} dt$. That choice is based partly on the analysis presented in Figure 2. In this figure we show the correlation between high time resolution magnetic indices and the ϵ parameter averaged over increasingly large windows, ranging from 1 to 60 min. The correlation increases monotonically in all cases, except for the case of the PC index. This increase is attributed to all the three effects described in the previous paragraph. The increase tends to be steepest prior to ~ 20 min.

[5] and strictly speaking also the F10.7 index, although it is assumed to be much less important at high latitudes

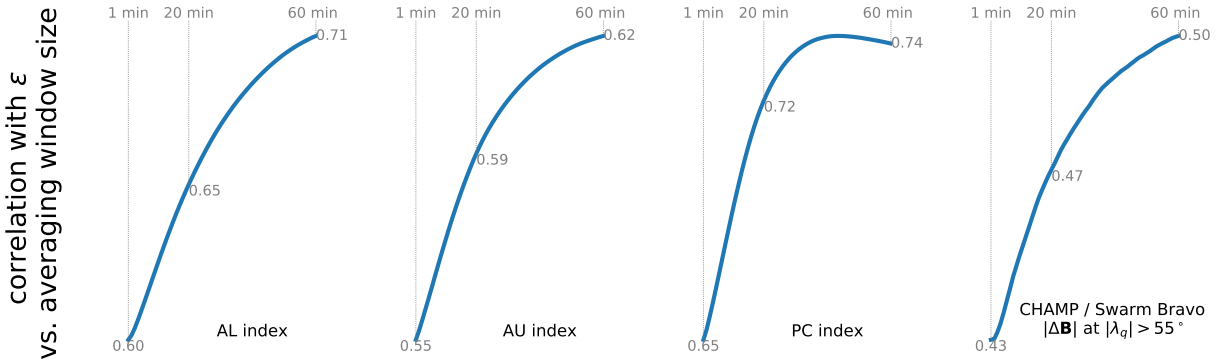

Figure 2: Plots of the Pearson correlation coefficient of four different parameters, at 1 min time resolution, with the Newell et al. [2007] ϵ (equation 10) coupling function as a function of averaging window size for ϵ. The temporal averaging is applied only to ϵ. Correlation coefficients at three different averaging window sizes are indicated in each plot. The indices and solar wind data come from the OMNI database. The $\|\Delta\mathbf{B}\|$ values used in the right plot are from CHAMP/*Swarm* Bravo 1 Hz data, sampled at 1 min cadence, in the region poleward of 55°. The plot is based on the period 2000−2016.

3 Currents and ground perturations

In this section we describe 1) how the ionospheric currents can be calculated from the model parameters, and 2) an approach for calculating the magnetic field perturbation on ground that are associated with the ionospheric currents. The currents are calculated at the height h_R, which is also the reference height in the modified apex coordinate system. At this height, $\lambda_q = \lambda_m$, so we skip the subscripts. We also use ϕ instead of $\phi_{\rm mlt}$. We give the units for each quantity, assuming that μ_0 is provided in units of Tm/A, and R_E, h_R in units of km. The spherical harmonic coefficients have units nT.

The currents are evaluated at $h = h_R$. They are essentially calculated from $\nabla\times\Delta\mathbf{B}/\mu_0$, treating the apex coordinates as orthogonal spherical, and $h + R_E$ as the geocentric radius.

The vertical current density (unit μA/m^2) is:

$$J_u(\lambda,\phi) = -\frac{10^{-6}}{\mu_0(R_E+h_R)}\sum_{n,m} n(n+1)P_n^m(\theta)\left[\psi_n^m\cos m\phi + \eta_n^m \sin m\phi\right]$$

The horizontal sheet current density is:

$$\mathbf{J} = \mathbf{J}_{df} + \mathbf{J}_{cf} = \mathbf{k}\times\nabla\Psi + \nabla\alpha, \tag{16}$$

where we have written $\mathbf{J}_{df}$ in terms of a scalar field Ψ, and $\mathbf{J}_{cf}$ in terms of a scalar field α. $\mathbf{k}$ is an upward unit vector.

The scalar for the divergence-free part Ψ (unit μA) is:

$$\Psi(\lambda,\phi) = -\frac{R_E}{\mu_0}\sum_{n,m}\frac{2n+1}{n}\left(\frac{R_E}{R_E+h_R}\right)^{n+1} P_n^m(\theta)\left[g_n^m\cos m\phi + h_n^m\sin m\phi\right] \tag{17}$$

This equation for Ψ corresponds to an equivalent current function of internal origin, as described in Chapman and Bartels [1940].

The scalar for the curl-free part α (unit μA) is[6]:

$$\alpha(\lambda,\phi) = -\frac{R_E + h_R}{\mu_0} \sum_{n,m} P_n^m(\theta)\,[\psi_n^m \cos m\phi_{\mathrm{mlt}} + \eta_n^m \sin m\phi] \tag{18}$$

From (16), we get the following expressions for the eastward and northward components of $\mathbf{J}_{df}$ and $\mathbf{J}_{cf}$ (unit mA/m):

$$J_{df,e} = -\frac{10^{-6}}{\mu_0} \sum_{n,m} \left(\frac{R_E}{R_E + h_R}\right)^{n+2} \frac{2n+1}{n} \frac{dP_n^m(\theta)}{d\theta} [g_n^m \cos(m\phi) + h_n^m \sin(m\phi)] \tag{19}$$

$$J_{df,n} = \frac{10^{-6}}{\mu_0 \cos\lambda} \sum_{n,m} \left(\frac{R_E}{R_E + h_R}\right)^{n+2} \frac{2n+1}{n} P_n^m(\theta) m [g_n^m \sin(m\phi) - h_n^m \cos(m\phi)] \tag{20}$$

$$J_{cf,e} = \frac{10^{-6}}{\mu_0 \cos\lambda} \sum_{n,m} P_n^m(\theta) m [\psi_n^m \sin(m\phi) - \eta_n^m \cos(m\phi)] \tag{21}$$

$$J_{cf,n} = \frac{10^{-6}}{\mu_0} \sum_{n,m} \frac{dP_n^m(\theta)}{d\theta} [\psi_n^m \cos(m\phi) + \eta_n^m \sin(m\phi)] \tag{22}$$

The total horizontal eastward current is (19) + (21), and the northward horizontal current is (20) + (22).

3.1 Corresponding ground magnetic field perturbations

By making some simple assumptions it is possible to calculate ground magnetic field perturbations from the model coefficients. The first assumption is that the equivalent current function Ψ (17) is equal to an equivalent current function associated with the external part of the magnetic potential at ground, as defined by Chapman and Bartels [1940]: First, we express the perturbation magnetic field below the ionosphere as $\Delta\mathbf{B} = -\nabla V$ where

$$V = R_E \sum_{n,m} P_n^m(\theta) \Bigg[\left(a_{n,e}^m \left(\frac{r}{R_E}\right)^n + a_{n,i}^m \left(\frac{R_E}{r}\right)^{n+1} \right) \cos(m\phi) + \left(b_{n,e}^m \left(\frac{r}{R_E}\right)^n + b_{n,i}^m \left(\frac{R_E}{r}\right)^{n+1} \right) \sin(m\phi) \Bigg]. \tag{23}$$

The subscripts of the Gauss coefficients, e and i, indicate if the associated field is of external or internal origin, respectively. The external field coefficients correspond to a current at $r = R_E + h_R$, $\mathbf{j}'_{df} = \hat{\mathbf{r}} \times \nabla\Psi'$, where

$$\Psi' = -\frac{R_E}{\mu_0} \sum_{n,m} \frac{2n+1}{n+1} \left(\frac{R_E + h_R}{R_E}\right)^n P_n^m(\lambda_q) \Big[a_{n,e}^m \cos(m\phi) + b_{n,e}^m \sin(m\phi) \Big]. \tag{24}$$

[6] There is a sign error in the corresponding equation (22) in Laundal et al. [2016] which has been corrected here

By assuming that $\Psi = \Psi'$ (equation 17 = equation 24) we find how $a^m_{n,e}$ and $b^m_{n_e}$ relate to g^m_n and h^m_n. Using these relationships, and (23), we find the expression for the associated ground perturbations. At $r = R_E$, they are (unit nT):

$$\Delta B_e = -\frac{1}{\cos\lambda}\sum_{n,m}\left(\frac{R_E}{R_E+h_R}\right)^{2n+1}\frac{n+1}{n}P^m_n(\theta)m[g^m_n\sin(m\phi) - h^m_n\cos(m\phi)] \tag{25}$$

$$\Delta B_n = -\sum_{n,m}\left(\frac{R_E}{R_E+h_R}\right)^{2n+1}\frac{n+1}{n}\frac{dP^m_n(\theta)}{d\theta}[g^m_n\cos(m\phi) + h^m_n\sin(m\phi)] \tag{26}$$

$$\Delta B_u = \sum_{n,m}\left(\frac{R_E}{R_E+h_R}\right)^{2n+1}(n+1)P^m_n(\theta)[g^m_n\cos(m\phi) + h^m_n\sin(m\phi)] \tag{27}$$

Some things to consider about these expressions:

- The eastward and northward magnetic field components should be treated as being equivalent to what Richmond [1995] calls $\Delta B_{q\phi}$ and $\Delta B_{q\lambda}$, respectively (equations 7.12 and 7.13 in that paper)
- The equations are evaluated at $r = R_E$. To keep r as a free parameter (at $< R_E+h_R$), multiply by $r^n R_E^{-n}$ in the horizontal components, and by $r^{n-1}R_E^{1-n}$ in the vertical component.
- We have made an assumption about the current sheet height, h_R. Our default value for this is 110 km. Increasing it decreases the associated magnetic field perturbation on ground.
- We have essentially neglected the internal induced field, in practice assuming that it is zero. Other assumptions are certainly possible to make, possibly improving ground magnetic field predictions.

Finally, we emphasize that the ambiguity/freedom in predicting ground magnetic field perturbations is not present in space, above the current sheet. There the model magnetic field components are given in terms of equations 4–6.

References

K. M. Laundal, C. C. Finlay, and N. Olsen. Sunlight effects on the 3D polar current system determined from low Earth orbit measurements. *Earth Planets Space*, 2016. doi: 10.1186/s40623-016-0518-x.

G. Backus. Poloidal and toroidal fields in geomagnetic field modeling. *Rev. Geophys.*, 24:75–109, 1986.

N. Olsen. Ionospheric F region currents at middle and low latitudes estimated from Magsat data. *J. Geophys. Res.*, 102:4563–4576, 1997.

A. D. Richmond. Ionospheric electrodynamics using magnetic apex coordinates. *J. Geomag. Geoelectr.*, 47:191–212, 1995.

K. M. Laundal and A. D. Richmond. Magnetic Coordinate Systems. *Space Sci. Rev.*, 2017. doi: 10.1007/s11214-016-0275-y.

J. T. Emmert, A. D. Richmond, and D. P. Drob. A computationally compact representation of Magnetic Apex and Quasi Dipole coordinates with smooth base vectors. *Journal of Geophysical Research: Space Physics*, 115(A8), 2010. doi: 10.1029/2010JA015326.

P. T. Newell, T. Sotirelis, K. Liou, C. I. Meng, and F. J. Rich. A nearly universal solar wind-magnetosphere coupling function inferred from 10 magnetospheric state variables. *J. Geophys. Res.*, 112, 2007. doi: 10.1029/2006JA012015.

C. C. Finlay, N. Olsen, S. Kotsiaros, N. Gillet, and L. Tøffner-Clausen. Recent geomagnetic secular variation from Swarm and ground observatories as estimated in the CHAOS-6 geomagnetic field model. *Earth, Planets and Space*, 68:112, 2016. doi: 10.1186/s40623-016-0486-1.

E. Anderson, Z. Bai, C. Bischof, S. Blackford, J. Demmel, J. Dongarra, J. Du Croz, A. Greenbaum, S. Hammarling, A. McKenney, and D. Sorensen. *LAPACK Users' Guide*. Society for Industrial and Applied Mathematics, Philadelphia, PA, third edition, 1999. ISBN 0-89871-447-8 (paperback).

P. J. Huber. Robust estimation of location parameter. *Ann. Math. Stat.*, 35:73–101, 1964.

D. R. Weimer. An empirical model of ground-level geomagnetic perturbations. *Space Weather*, 11: 107–120, 2013. doi: 10.1002/swe.20030.

S. Chapman and J. Bartels. *Geomagnetism Vol. II*. Oxford University Press, London, UK, 1940.